# Sum-frequency phonon spectroscopy on $\alpha$-quartz

Wei-Tao Liu and Y. R. Shen*
*Physics Department, University of California at Berkeley, Berkeley, California 94720, USA*
(Received 14 March 2008; published 23 July 2008)

We demonstrate here, using $\alpha$-quartz as an example, that IR-visible sum-frequency (SF) spectroscopy can be employed to probe zone-center optical phonons of crystals without inversion symmetry. Because only modes both IR and Raman active are allowed in the SF process, the observed phonon spectrum is greatly simplified. The intrinsic flexibility of SF spectroscopy also permits more accurate determination of relative magnitudes and signs of relevant Raman polarizabilities.

DOI: 10.1103/PhysRevB.78.024302 PACS number(s): 63.20.−e, 78.20.−e

## I. INTRODUCTION

Zone-center optical phonons of a crystal are important characteristics of the crystalline structure. They are usually studied with IR and Raman spectroscopy techniques, which provide complementary information about the phonons. Recently, IR-visible sum-frequency spectroscopy has become increasingly popular.[1] It is obvious that sum-frequency (SF) spectroscopy can also be used to probe phonons if the IR input is tunable over phonon resonances. However, only a few phonon-related SF studies exist so far[2,3] and they are not concerned with investigation of phonon properties. We report here a study on $\alpha$-quartz to demonstrate the capability of SF spectroscopy to study phonons.

Sum-frequency generation (SFG) is a second-order nonlinear optical process in which two input pulses of different frequencies overlap in a medium and generate an output at the sum frequency.[4] When the IR input tunes over a phonon resonance, the SF output exhibits accordingly a resonant enhancement [Fig. 1(a)]. This then leads to a spectrum for the zone-center optical phonons. By symmetry, SFG is only allowed in crystals without inversion symmetry and resonantly enhanced only with phonon modes that are both IR and Raman active.[4] The latter helps simplify the detected spectrum, which can be an advantage in assigning phonon modes in the spectrum of a crystal that is highly congested. That the polarizations of input and output beams are independently adjustable in SFG also helps. It facilitates symmetry identification and characterization of the phonon modes and permits accurate determination of relative magnitudes and signs of their Raman polarizabilities.

To demonstrate SF spectroscopic study of phonons, we used $\alpha$-quartz as an example. The zone-center phonon properties of $\alpha$-quartz have been well studied by IR and Raman spectroscopies, showing that only modes belong to the $E$ representation are both IR and Raman active.[5–7] The $E$ phonons appeared clearly in our SF spectra, and their characteristics matched well with those deduced from IR and Raman measurements. Our results, however, provide much better accuracy in determination of relative magnitudes and signs of the relevant Raman polarizability elements. This case illustrates that SF phonon spectroscopy can provide useful complementary information to IR and Raman spectroscopies in studies of phonons of noncentrosymmetric crystals.

## II. THEORETICAL BACKGROUND

The basic theory of IR-visible SF spectroscopy is well established.[8] We focus here on SFG in reflection from a sample depicted in Fig. 1(b). A visible beam at fixed frequency $\omega_{\mathrm{vis}}$ and a tunable IR beam at frequency $\omega_{\mathrm{IR}}$ overlapping on the sample generate a SF signal $S(\omega_{\mathrm{SF}}=\omega_{\mathrm{vis}}+\omega_{\mathrm{IR}})$ in the reflected direction. We consider media without inversion symmetry, for which the surface contribution to SFG is generally negligible. In terms of the bulk nonlinear susceptibility, $\vec{\vec{\chi}}^{(2)}$ the signal is given by

$$S(\omega_{\mathrm{SF}}) \propto |(\hat{e}_{\mathrm{SF}}\vec{\vec{L}}_{\mathrm{SF}}) \cdot \vec{\vec{\chi}}^{(2)}:(\vec{\vec{L}}_{\mathrm{vis}} \cdot \hat{e}_{\mathrm{vis}})(\vec{\vec{L}}_{\mathrm{IR}} \cdot \hat{e}_{\mathrm{IR}})/\Delta k|^2. \quad (1)$$

Here $\vec{\vec{L}}_n$ is the tensorial Fresnel transmission coefficient at $\omega_n$, $\hat{e}_n$ is the unit polarization vector of the beam at $\omega_n$, and $\Delta k \equiv |\vec{k}(\omega_{\mathrm{SF}})-\vec{k}(\omega_{\mathrm{vis}})-\vec{k}(\omega_{\mathrm{IR}})|$ is the wave vector mismatch of SFG with $\vec{k}(\omega_n)$ denoting the *complex* wave vector at $\omega_n$ in the medium.[4] The Fresnel coefficients in the laboratory coordinates $(x,y,z)$ with $z$ along the surface normal and $x$-$z$ defining the incidence plane have the expressions,[9]

$$L_{xx}(\omega_n) = \frac{2k_z(\omega_n)}{\varepsilon(\omega_n)k_{0z}(\omega_n)+k_z(\omega_n)},$$

$$L_{yy}(\omega_n) = \frac{2k_{0z}(\omega_n)}{k_{0z}(\omega_n)+k_z(\omega_n)},$$

$$L_{zz}(\omega_n) = \frac{2k_{0z}(\omega_n)}{\varepsilon(\omega_n)k_{0z}(\omega_n)+k_z(\omega_n)}, \quad (2)$$

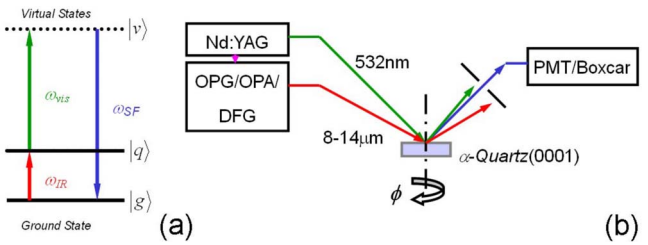


FIG. 1. (Color online) (a) Energy level diagram illustrating the SF process. (b) Schematics of the experimental arrangement for SF spectroscopy.

 

where $\varepsilon$ and $k_0$ refer to the dielectric constant of the medium and wave vector in air, respectively. The nonlinear susceptibility $\vec{\chi}^{(2)}$ is a characteristic of the medium. As $\omega_{\mathrm{IR}}$ approaches an optical phonon resonance, $\vec{\chi}^{(2)}$ is resonantly enhanced. For discrete resonances, it can be expressed as[8]

$$\vec{\chi}^{(2)} = \vec{\chi}^{(2)}_{NR} + \sum_q \frac{\vec{A}^{(2)}_q}{\omega_{IR} - \omega_q + i\Gamma_q}, \tag{3}$$

with $\vec{\chi}^{(2)}_{\mathrm{NR}}$ being the nonresonant contribution, and $\vec{A}^{(2)}_q$, $\omega_q$, and $\Gamma_q$ denoting the amplitude, resonant frequency, and the damping coefficient of the $q$th resonance, respectively.

We are interested in studying optical phonons of $\alpha$-quartz, which has rhombohedral structure of point-group symmetry $D_3$ (32).[10] Its $\vec{\chi}^{(2)}$ tensor has in general the following nonvanishing elements:[4]

$$\chi^{(2)}_{aaa} = -\chi^{(2)}_{abb} = -\chi^{(2)}_{bba} = -\chi^{(2)}_{bab},$$

$$\chi^{(2)}_{abc} = -\chi^{(2)}_{bac}, \quad \chi^{(2)}_{acb} = -\chi^{(2)}_{bca} \quad \text{and} \quad \chi^{(2)}_{cab} = -\chi^{(2)}_{cba}, \tag{4}$$

where $(a,b,c)$ denotes the set of principal axes with $c$ and $a$ parallel to the threefold and twofold axes, respectively. The $\vec{\chi}^{(2)}$ elements expressed in the laboratory coordinates $(x,y,z)$ are related to those in the crystal coordinates $(a,b,c)$ by

$$\chi^{(2)}_{ijk} = \sum\nolimits_{lmn} \chi^{(2)}_{lmn} (\hat{i}\cdot\hat{l})(\hat{j}\cdot\hat{m})(\hat{k}\cdot\hat{n}). \tag{5}$$

In our experiment, we oriented $\alpha$-quartz with the $c$ axis along $z$, and the $\alpha$ axis at an angle $\phi_0$ away from the $x$-$z$ plane. We then have $\hat{a} = \cos\phi_0\hat{x} + \sin\phi_0\hat{y}$, $\hat{b} = -\sin\phi_0\hat{x} + \cos\phi_0\hat{y}$, and $\hat{c} = \hat{z}$, and the nonvanishing elements in the laboratory coordinates are

$$\chi^{(2)}_{xxx} = -\chi^{(2)}_{xyy} = -\chi^{(2)}_{yxy} = -\chi^{(2)}_{yyx} = \chi^{(2)}_{aaa}\cos 3\phi_0,$$

$$\chi^{(2)}_{xxy} = \chi^{(2)}_{xyx} = \chi^{(2)}_{yxx} = -\chi^{(2)}_{yyy} = \chi^{(2)}_{aaa}\sin 3\phi_0,$$

$$\chi^{(2)}_{xyz} = -\chi^{(2)}_{yxz} = \chi^{(2)}_{abc},$$

$$\chi^{(2)}_{xzy} = -\chi^{(2)}_{yzx} = \chi^{(2)}_{acb} \quad \text{and} \quad \chi^{(2)}_{zxy} = -\chi^{(2)}_{zyx} = \chi^{(2)}_{cab}. \tag{6}$$

With $x$-$z$ taken as the plane of incidence, measurements using polarization combinations SSS (denoting S-, S-, and S-polarized SF output, visible input, and IR input, respectively), SPP and PSP yield SF signals,

$$S_{\mathrm{SSS}}(\omega_{\mathrm{SF}}) \propto |L_{yy}(\omega_{\mathrm{SF}})\chi^{(2)}_{yyy}L_{yy}(\omega_{\mathrm{vis}})L_{yy}(\omega_{\mathrm{IR}})/\Delta k|^2,$$

$$\begin{aligned} S_{\mathrm{SPP}}(\omega_{\mathrm{SF}}) \propto |&L_{yy}(\omega_{\mathrm{SF}})\chi^{(2)}_{yxx}\cos\theta_{\mathrm{vis}}L_{xx}(\omega_{\mathrm{vis}})\cos\theta_{\mathrm{IR}}L_{xx}(\omega_{\mathrm{IR}}) + L_{yy}(\omega_{\mathrm{SF}})\chi^{(2)}_{yxz}\cos\theta_{\mathrm{vis}}L_{xx}(\omega_{\mathrm{vis}})\sin\theta_{\mathrm{IR}}L_{zz}(\omega_{\mathrm{IR}}) \\ &+ L_{yy}(\omega_{\mathrm{SF}})\chi^{(2)}_{yzx}\sin\theta_{\mathrm{vis}}L_{zz}(\omega_{\mathrm{vis}})\cos\theta_{\mathrm{IR}}L_{xx}(\omega_{\mathrm{IR}}) + L_{yy}(\omega_{\mathrm{SF}})\chi^{(2)}_{yzz}\sin\theta_{\mathrm{vis}}L_{zz}(\omega_{\mathrm{vis}})\sin\theta_{\mathrm{IR}}L_{zz}(\omega_{\mathrm{IR}})|^2/\Delta k^2, \end{aligned}$$

$$\begin{aligned} S_{\mathrm{PSP}}(\omega_{\mathrm{SF}}) \propto |&-\cos\theta_{\mathrm{SF}}L_{xx}(\omega_{\mathrm{SF}})\chi^{(2)}_{xyx}L_{yy}(\omega_{\mathrm{vis}})\cos\theta_{\mathrm{IR}}L_{xx}(\omega_{\mathrm{IR}}) - \cos\theta_{\mathrm{SF}}L_{xx}(\omega_{\mathrm{SF}})\chi^{(2)}_{xyz}L_{yy}(\omega_{\mathrm{vis}})\sin\theta_{\mathrm{IR}}L_{zz}(\omega_{\mathrm{IR}}) \\ &+ \sin\theta_{\mathrm{SF}}L_{zz}(\omega_{\mathrm{SF}})\chi^{(2)}_{zyx}L_{yy}(\omega_{\mathrm{vis}})\cos\theta_{\mathrm{IR}}L_{xx}(\omega_{\mathrm{IR}}) + \sin\theta_{\mathrm{SF}}L_{zz}(\omega_{\mathrm{SF}})\chi^{(2)}_{zyz}L_{yy}(\omega_{\mathrm{vis}})\sin\theta_{\mathrm{IR}}L_{zz}(\omega_{\mathrm{IR}})|^2/\Delta k^2, \end{aligned} \tag{7}$$

where $\theta_n$ is the incident angle of the $\omega_n$ beam. From measurements with different $\phi_0$ and polarization combinations, we can deduce the nonvanishing $\chi^{(2)}_{lmn}$ using Eqs. (6) and (7).

The characteristics of resonances, $\vec{A}^{(2)}_q$, $\omega_q$, and $\Gamma_q$, can be obtained by fitting an observed spectrum with Eqs. (3) and (7). Because the SFVS process is a combination of IR and Raman excitations [Fig. 1(a)], the resonant amplitude $A^{(2)}_{q,lmn}$ can be expressed as[4,8,9]

$$\begin{aligned} A^{(2)}_{q,lmn} &\propto \sum_v \left( \frac{\langle g|\mu_l|v\rangle\langle v|\mu_m|q\rangle}{\omega_{\mathrm{SF}} - \omega_{\mathrm{vg}} + i\Gamma_{\mathrm{vg}}} - \frac{\langle v|\mu_l|q\rangle\langle g|\mu_m|v\rangle}{\omega_{\mathrm{SF}} - \omega_{\mathrm{qv}} + i\Gamma_{\mathrm{qv}}} \right) \\ &\quad \times \langle q|\mu_n|g\rangle \\ &\propto \frac{1}{\omega_q}\frac{\partial\alpha^{(1)}_{lm}}{\partial Q_q}\frac{\partial\mu_n}{\partial Q_q}, \end{aligned} \tag{8}$$

where $Q_q$ the normal-mode coordinate, $\vec{\mu}$ is the dipole moment, $\partial\mu_n/\partial Q_q$ and $\partial\alpha^{(1)}_{lm}/\partial Q_q$ are the IR dipole derivative and Raman polarizability of the $q$th mode, and $|g\rangle$, $|q\rangle$, and $|v\rangle$ refer to the ground, phonon, and virtual states, respectively.[8] As characteristic of the crystal, $A^{(2)}_{q,lmn}$ and $A^{(2)}_{q,ijk}$ should satisfy the symmetry relations given in Eqs. (4) and (6) for $\chi^{(2)}_{lmn}$ and $\chi^{(2)}_{ijk}$. In addition, they also vanish if the mode cannot be both IR and Raman excited, i.e., $\partial\mu_n/\partial Q_q = 0$ or $\partial\alpha^{(1)}_{lm}/\partial Q_q = 0$. This happens in the case of $\alpha$-quartz for all zone-center phonon modes except the $E$ modes, and even for $E$ modes if the IR excitation does not have a polarization component perpendicular to the $c$ axis.[11] Thus the only nonvanishing elements of $A^{(2)}_{q,lmn}$ for $E$ phonon modes of $\alpha$-quartz are $A^{(2)}_{q,aaa} = -A^{(2)}_{q,abb} = -A^{(2)}_{q,bba} = -A^{(2)}_{q,bab}$, $A^{(2)}_{q,bca} = -A^{(2)}_{q,acb}$, and $A^{(2)}_{q,cba} = -A^{(2)}_{q,cab}$. With both $\omega_{\mathrm{vis}}$ and $\omega_{\mathrm{SF}}$ far away from resonances, we further expect $A^{(2)}_{q,bca} \approx A^{(2)}_{q,cba}$.[8,9] These elements can be deduced from the measured spectra with polarization combinations, SSS, SPP, and PSP, described in Eq. (7). Explicitly, from Eqs. (3), (6), and (7), we have for SSS, SPP, and PSP measurements that

$$S_{\mathrm{SSS}} \propto \left| L_{yy}(\omega_{\mathrm{SF}})L_{yy}(\omega_{\mathrm{vis}})L_{yy}(\omega_{\mathrm{IR}}) \cdot \left( \chi^{(2)}_{\mathrm{NR},aaa} + \sum_q \frac{A^{(2)}_{q,aaa}}{\omega_{\mathrm{IR}} - \omega_q + i\Gamma} \right) \sin 3\phi_0 \right|^2 / \Delta k^2,$$

$$\begin{aligned} S_{\mathrm{SPP}} \propto \Bigg| & L_{yy}(\omega_{\mathrm{SF}})\cos\,\theta_{\mathrm{vis}} L_{xx}(\omega_{\mathrm{vis}})\cos\,\theta_{\mathrm{IR}} L_{xx}(\omega_{\mathrm{IR}}) \cdot \left[ \chi^{(2)}_{\mathrm{NR},aaa} + \sum_q \frac{A^{(2)}_{q,aaa}}{\omega_{\mathrm{IR}} - \omega_q + i\Gamma_q} \right] \sin 3\phi_0 \\ & - L_{yy}(\omega_{\mathrm{SF}})\cos\,\theta_{\mathrm{vis}} L_{xx}(\omega_{\mathrm{vis}})\sin\,\theta_{\mathrm{IR}} L_{zz}(\omega_{\mathrm{IR}}) \cdot \chi^{(2)}_{\mathrm{NR},abc} \\ & + L_{yy}(\omega_{\mathrm{SF}})\sin\,\theta_{\mathrm{vis}} L_{zz}(\omega_{\mathrm{vis}})\cos\,\theta_{\mathrm{IR}} L_{xx}(\omega_{\mathrm{IR}}) \cdot \left[ \chi^{(2)}_{\mathrm{NR},bca} + \sum_q \frac{A^{(2)}_{q,bca}}{\omega_{\mathrm{IR}} - \omega_q + i\Gamma_q} \right] \Bigg|^2 \Delta k^2, \end{aligned} \tag{9}$$

$$\begin{aligned} S_{\mathrm{PSP}} \propto \Bigg| & -\cos\,\theta_{\mathrm{SF}} L_{xx}(\omega_{\mathrm{SF}})L_{yy}(\omega_{\mathrm{vis}})\cos\,\theta_{\mathrm{IR}} L_{xx}(\omega_{\mathrm{IR}}) \cdot \left[ \chi^{(2)}_{\mathrm{NR},aaa} + \sum_q \frac{A^{(2)}_{q,aaa}}{\omega_{\mathrm{IR}} - \omega_q + i\Gamma_q} \right] \sin 3\phi_0 \\ & - \cos\,\theta_{\mathrm{SF}} L_{xx}(\omega_{\mathrm{SF}})L_{yy}(\omega_{\mathrm{vis}})\sin\,\theta_{\mathrm{IR}} L_{zz}(\omega_{\mathrm{IR}}) \cdot \chi^{(2)}_{\mathrm{NR},abc} \\ & + \sin\,\theta_{\mathrm{SF}} L_{zz}(\omega_{\mathrm{SF}})L_{yy}(\omega_{\mathrm{vis}})\cos\,\theta_{\mathrm{IR}} L_{xx}(\omega_{\mathrm{IR}}) \cdot \left[ \chi^{(2)}_{\mathrm{NR},cba} + \sum_q \frac{A^{(2)}_{q,cba}}{\omega_{\mathrm{IR}} - \omega_q + i\Gamma_q} \right] \Bigg|^2 / \Delta k^2. \end{aligned}$$

These equations show that fitting of the SSS, SPP, and PSP spectra allow us to deduce the resonant characteristics of the $E$ phonon modes of quartz, in particular, the resonant amplitudes $A^{(2)}_{q,aaa}$, $A^{(2)}_{q,bca}$, and $A^{(2)}_{q,cba}$.

## III. EXPERIMENTAL ARRANGEMENT

Our experimental setup, depicted in Fig. 1(b), was similar to that of Ref. 8. Both the visible input (~500 $\mu$J/pulse) at 532 nm and the IR input (~30 $\mu$J/pulse in average) tunable from ~8 to 14 $\mu$m were derived from a 20 ps Nd doped yttrium aluminum garnet and optical parametric system. The two beams overlapped on a 5-mm-thick $\alpha$-quartz slab (from Princeton Scientific Corp.) with incident angles of 45° and 57° respectively, and spots size of ~200 $\mu$m. The SF output was detected in the reflected direction using a photomultiplier and gate integrator system, and the spectra were normalized to those from a GaAs(110) wafer. The sample was mounted on a rotatory stage that allowed azimuthal rotation of the sample about its $c$ axis (also the surface normal). Measurements were performed at room temperature.

## IV. RESULTS AND ANALYSES

Figures 2(a) and 2(b) present the SSS and SPP SF phonon spectra of $\alpha$-quartz taken at various $\phi_0$ in the 750–1300 cm$^{-1}$ range. The PSP spectra are nearly the same as that of SPP with $\phi_0 \rightarrow -\phi_0$. Three resonant modes, at 795, 1064, and 1160 cm$^{-1}$, are clearly observed in the spectra. They can be attributed to the zone-center TO phonons that belong to the $E$ irreducible representation of the $D_3$ symmetry group, following the assignment in earlier experimental[5–7] and theoretical[10] studies on $\alpha$-quartz. In this frequency regime, modes belonging to other irreducible representations, namely, the $A_1$ modes at ~780 and 1080 cm$^{-1}$ and $A_2$ mode at ~1070 cm$^{-1}$,[5–7,10] are not observed because they are not both IR and Raman active. The LO phonons of the $E$ modes[5–7,10] are not observed either because they cannot be excited by the transverse IR field.

We can fit the spectra in Fig. 2 using Eq. (9) to deduce the resonant characteristics of the $E$ modes of $\alpha$-quartz. For the fit, however, we need to know $L_{ii}(\omega_{\mathrm{IR}})$ and $\Delta k(\omega_{\mathrm{IR}})$. They can be obtained from the known linear dielectric constants of $\alpha$-quartz[5] and are plotted in Fig. 3. The strong dispersion of the linear dielectric constant near phonon resonances leads to the strong dispersions of $L_{ii}(\omega_{\mathrm{IR}})$ and $\Delta k(\omega_{\mathrm{IR}})$. In particular, $|L_{ii}(\omega_{\mathrm{IR}})|^2$ can change by orders of magnitude across a Restrahl band and drastically affect the SF resonant profiles. With $L_{ii}(\omega_{\mathrm{IR}})$ and $\Delta k(\omega_{\mathrm{IR}})$ known, we can fit the SF spectra very well using Eq. (9), as shown by the solid lines in Fig. 2. The deduced resonant frequencies, amplitudes (normalized to the 1160 cm$^{-1}$ mode), and damping constants for the three phonons modes are listed in Table I. We also found $A^{(2)}_{q,bca} \approx A^{(2)}_{q,cba}$ for all three resonant modes. We note that for the nonresonant part, $\chi^{(2)}_{\mathrm{NR},aaa} \approx 0.09$ (normalized to $A^{(2)}_{q,aaa}/\Gamma_q$ of the 1160 cm$^{-1}$ mode) and $\chi^{(2)}_{\mathrm{NR},abc} \approx \chi^{(2)}_{\mathrm{NR},bca} \approx \chi^{(2)}_{\mathrm{NR},cba} \approx 0$.[12]

According to Eq. (9), we have $S_{\mathrm{SSS}} \propto \sin^2 3\phi_0$, exhibiting a sixfold azimuthal symmetry, and $S_{\mathrm{SPP}} \propto |A + B \sin 3\phi_0|^2$ and $S_{\mathrm{PSP}} \propto |A' + B' \sin 3\phi_0|$, exhibiting threefold azimuthal symmetries at given IR frequencies. With $\theta_{\mathrm{vis}} = 45°$ and $\theta_{\mathrm{SF}} \approx 45.5°$ in our experiment, we have $A \approx A'$ and $B \approx -B'$. Plotted in Figs. 4(a)–4(c) are measured $S_{\mathrm{SSS}}$ $S_{\mathrm{SPP}}$, and $S_{\mathrm{PSP}}$ signals versus $\phi_0$ at the three resonant frequencies. The results indeed show good agreement with the predicted expressions (solid curves in Fig. 4). Moreover, the many data points allow very accurate determination of the value of $A/B$, hence, $A^{(2)}_{q,bca}/A^{(2)}_{q,aaa}$ for each mode using Eq. (9), as listed in Table I.

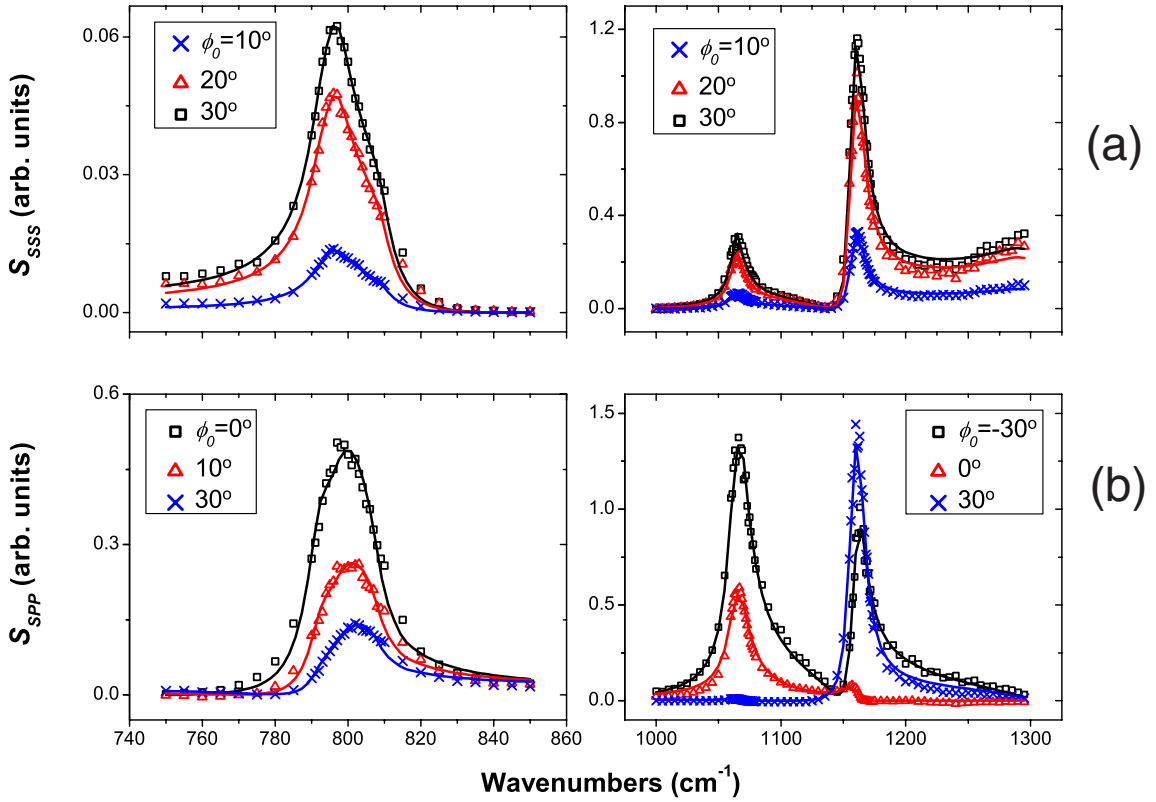


FIG. 2. (Color online) SF phonon spectra from $\alpha$-quartz with (a) SSS and (b) SPP beam polarization combinations for different azimuthal angles $\phi_0$. The solid lines are theoretical fits using Eq. (9).

## V. DISCUSSION

We have seen that SFVS allows fairly precise characterization of the $E$ phonon modes of $\alpha$-quartz. We can relate the results to those deduced from IR and Raman spectroscopy on $\alpha$-quartz. Equation (8) shows that the resonant amplitude $A^{(2)}_{q,lmn}$ is proportional to the product of IR dipole derivative $\partial\mu_n/\partial Q_q$ and Raman polarizability $\partial\alpha^{(1)}_{lm}/\partial Q_q$. For each $E$ phonon mode, we have the following nonvanishing elements of $\partial\vec{\mu}/\partial Q_q$ and $\partial\vec{\alpha}^{(1)}/\partial Q_q$:[5–7,11]

$$\partial\mu_a/\partial Q_q = \partial\mu_b/\partial Q_q,$$

$$\partial\alpha^{(1)}_{aa}/\partial Q_q = -\partial\alpha^{(1)}_{bb}/\partial Q_q = -\partial\alpha^{(1)}_{ab}/\partial Q_q = -\partial\alpha^{(1)}_{ba}/\partial Q_q,$$

$$\partial\alpha^{(1)}_{ac}/\partial Q_q = -\partial\alpha^{(1)}_{bc}/\partial Q_q = -\partial\alpha^{(1)}_{cb}/\partial Q_q = -\partial\alpha^{(1)}_{ca}/\partial Q_q.$$

With values of $|\partial\mu_a/\partial Q_q|$, $|\partial\alpha^{(1)}_{aa}/\partial Q_q|$, and $|\partial\alpha^{(1)}_{bc}/\partial Q_q|$ from IR (Ref. 5) and Raman[6,7] measurements reported in the literature, we can calculate $|A^{(2)}_{q,aaa}|$ from $A^{(2)}_{q,aaa} \propto (1/\omega_q)(\partial\alpha^{(1)}_{aa}/\partial Q_q)(\partial\mu_a/\partial Q_q)$ to compare with those we measured using SFVS. The comparison is given in of Table I (all normalized to the 1160 cm$^{-1}$ mode), showing fair agreement. The uncertainties in the calculated values mainly come from uncertainties in the Raman measurement. We also have $A^{(2)}_{q,bca}/A^{(2)}_{q,aaa} = (\partial\alpha^{(1)}_{bc}/\partial Q_q)/(\partial\alpha^{(1)}_{aa}/\partial Q_q)$, which allows us to compare the results from SF spectroscopy and Raman measurements. In Raman studies, this quantity is derived from the polarization dependence of the scattered Raman signals.[6,7] As shown in Table I, the agreement again is fair, with SFVS providing not only much better accuracy but also relative signs of $A^{(2)}_{q,bca}/A^{(2)}_{q,aaa}$ for different modes.

Generally, the SF vibrational spectra for a crystal are much simpler than IR and Raman spectra due to the more stringent selection rule that only phonon modes both IR and

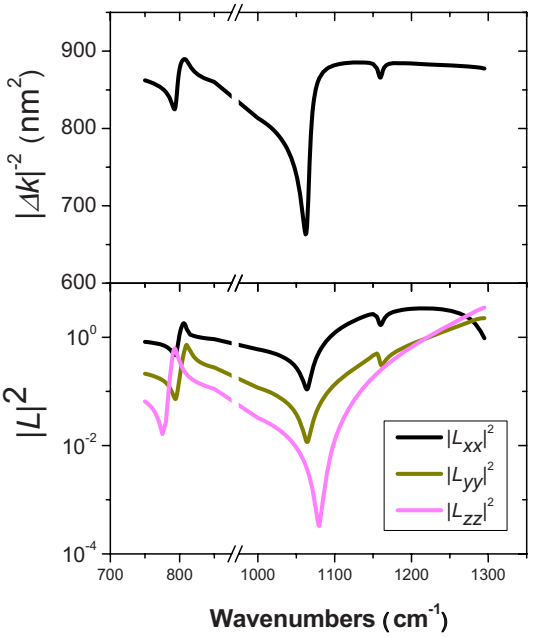


FIG. 3. (Color online) Calculated Fresnel coefficients and wave vector mismatch for SF reflection from $\alpha$-quartz.

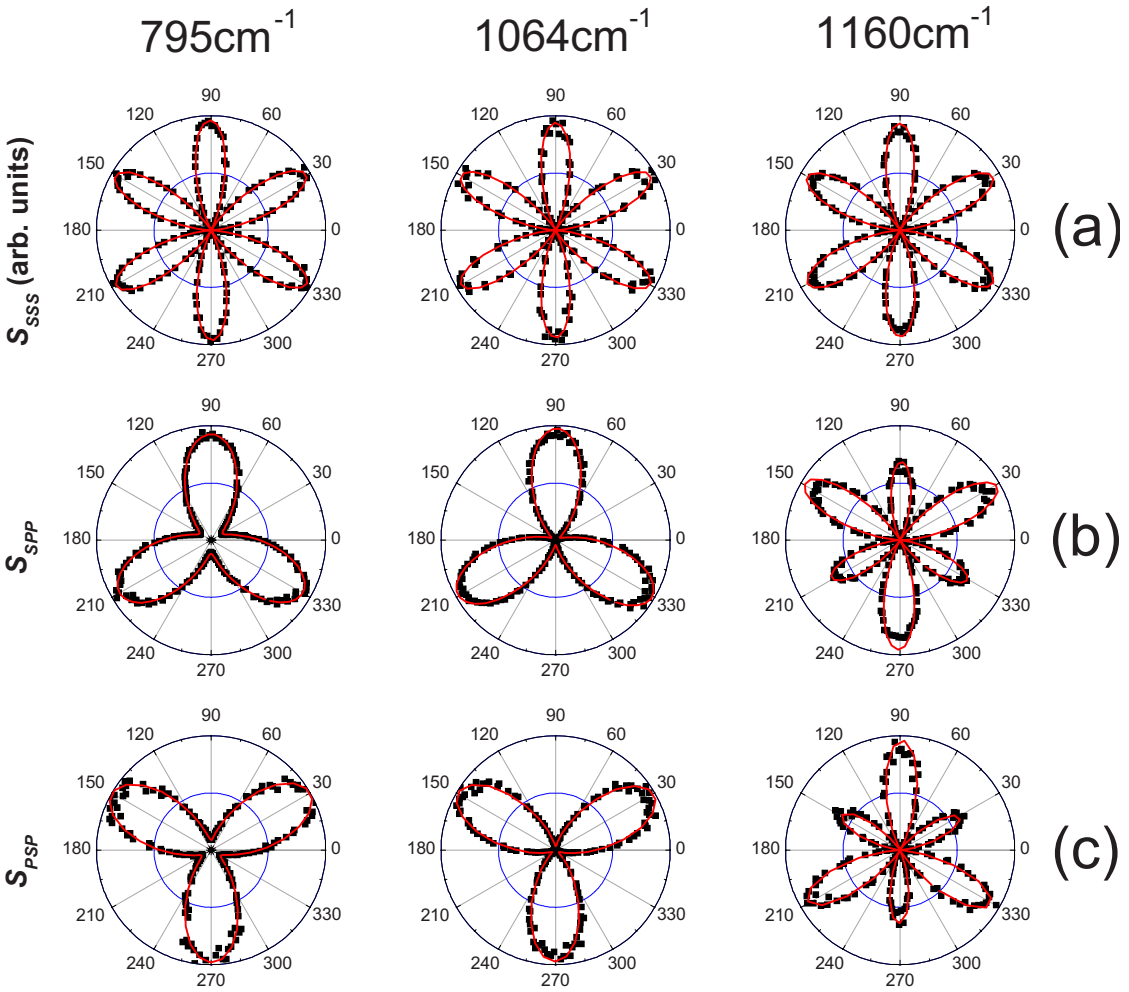


FIG. 4. (Color online) Azimuthal symmetry of SF signal at three phonon resonances with (a) SSS, (b) SPP, and (c) PSP polarization combinations. The solid lines are theoretical fits using Eq. (9).

Raman active are allowed. For example, only 3 out of 13 phonon modes of $\alpha$-quartz existing in the 750–1300 $cm^{-1}$ range[10] can be detected by SF spectroscopy. For complex materials showing highly congested phonon spectra, this feature would help the phonon assignment. It is also easy for SFG to distinguish the symmetry representations of the allowed phonon modes from the signal variation with respect to the sample orientation about the beam incident plane. Take crystals belonging to the $C_{3v}$ $(3m)$ point group as an example, for which both $A_1$ and $E$ phonons are allowed in SF spectroscopy.[11] With the threefold axis along the surface normal, the SSS polarization combination of SF spectroscopy only detects the $E$ modes with a sixfold azimuthal symmetry described by $S_{E,\mathrm{SSS}} \propto \sin^2 3\phi_0$, but not the $A_1$ modes. The latter show up in SSP, SPS, PSS, and PPP polarization combinations but have isotropic azimuthal symmetry about the

TABLE I. Columns 1–3: Resonant frequency $\omega_q$, damping coefficient $\Gamma_q$, and resonant amplitude $|A^{(2)}_{q,aaa}|$ (normalized to that of the 1160 $cm^{-1}$ mode) of each phonon deduced from fitting the observed SSS spectra using Eq. (9). Column 4: Ratio of $A^{(2)}_{q,bca}/A^{(2)}_{q,aaa}$ deduced from experiment (signs are relative to that of the 1160 $cm^{-1}$ mode). Columns 5 and 6: Values of $|A^{(2)}_{q,aaa}|$ and $A^{(2)}_{q,bca}/A^{(2)}_{q,aaa}$ calculated using parameters given in Refs. 5–7.

| $\omega_q$ ($cm^{-1}$) | $\Gamma_q$ ($cm^{-1}$) | $\lvert A^{(2)}_{q,aaa}\rvert$expt. | $A^{(2)}_{q,bca}/A^{(2)}_{q,aaa}$expt. | $\lvert A^{(2)}_{q,aaa}\rvert$calc. [a] | $\lvert A^{(2)}_{q,bca}/A^{(2)}_{q,aaa}\rvert$calc. |
|---|---|---|---|---|---|
| $795 \pm 2$ | $4.4 \pm 0.1$ | $0.9 \pm 0.1$ | $-(3.0 \pm 0.2)$ | $\sim 1.4$,[b] $<0.7$ [c] | $\sim 2.7$,[b] $>3.7$ [c] |
| $1064 \pm 2$ | $3.7 \pm 0.6$ | $2.3 \pm 0.1$ | $-(2.3 \pm 0.1)$ | $\sim 2.6$,[b] $<1.7$ [c] | $\sim 2.8$,[b] $>1.6$ [c] |
| $1160 \pm 2$ | $5.1 \pm 0.1$ | 1 | $0.4 \pm 0.1$ | 1 | 0.6,[b] 0.5[c] |

[a]With values of $\partial\mu_a/\partial Q_q$ in Ref. 5.
[b]With values of $\partial\alpha^{(1)}_{lm}/\partial Q_q$ in Ref. 6.
[c]With values of $\partial\alpha^{(1)}_{lm}/\partial Q_q$ in Ref. 7.

surface normal (independent of $\phi_0$). Thus the two modes can be easily distinguished in SFVS with different polarization combinations and sample rotations.

In characterizing phonons, SF phonon spectroscopy generally has more flexibility than IR and Raman spectroscopy. Because SFVS involves two input and one output beam, each with two independent beam polarizations, it can access a total of eight independent elements of $A^{(2)}_{q,ijk}$ with a given beam geometry [$(i,j,k)$ referring to the laboratory coordinates]. In contrast, IR and Raman spectroscopies can access only 2 and 4 of their respective elements, $\partial\mu_k/\partial Q_q$ and $\partial\alpha^{(1)}_{ij}/\partial Q_q$, with fixed beam geometry. Since changing beam geometry often introduces errors and uncertainties, this makes the determination of $A^{(2)}_{q,lmn}$ [$(l,m,n)$ referring to the crystalline axes] easier and more accurate. This is particularly true in comparison with Raman measurements of $\partial\alpha^{(1)}_{lm}/\partial Q_q$, as we have demonstrated here with $\alpha$-quartz. To determine accurately the ratio of different $\partial\alpha^{(1)}_{lm}/\partial Q_q$ in Raman measurements, for example, one generally needs a cube sample with all sides polished and the 90° scattered radiation collected in a limited angle through the two side surfaces.[7] If the crystal is linearly or circularly birefringent, the beam polarization could vary as it propagates in the crystal. This could cause further complication in IR and Raman measurements. SF generation from reflection, on the other hand, has no such difficulty because the effective interaction region is limited to $\Delta k^{-1}$, less than a reduced visible wavelength near the surface and within which the beam polarizations hardly change. This also suggests that compared to Raman spectroscopy it will be generally more convenient for SF spectroscopy to probe phonons of thin crystalline films. Moreover, as the conventional polarized Raman measurements yield only magnitudes of $\partial\alpha^{(1)}_{lm}/\partial Q_q$, SF spectroscopy can further provide information of their relative signs as demonstrated in our study.

## VI. CONCLUSION

We have used SF spectroscopy to probe zone-center phonons of $\alpha$-quartz in the 750–1300 $cm^{-1}$ range. Because only phonon modes that are both IR and Raman active are allowed in SF spectroscopy, the observed spectra are greatly simplified. Only transverse $E$ modes appear on the spectra of $\alpha$-quartz. This simplification could be advantageous in studies of crystals with more complex unit cells that could lead to more congested IR and Raman spectra. Being a second-order nonlinear optical process involving three separate beams, SF spectroscopy offers great flexibility in measurements. It can allow easy and accurate characterization of phonon properties, such as symmetry representation and relative magnitudes and signs of their Raman polarizability elements. What we describe here is generally true for crystals without inversion symmetry, and this work is a demonstration that SF phonon spectroscopy can be a useful complementary tool to study zone-center phonons of such crystals.

## ACKNOWLEDGMENTS

This work was supported by the Director, Office of Science, Office of Basic Energy Sciences, Materials Sciences and Engineering Division, U.S. Department of Energy under Contract No. DE-AC03-76SF00098.

*yrshen@calmail.berkeley.edu

[1] M. B. Raschke and Y. R. Shen, Curr. Opin. Solid State Mater. Sci. **8**, 343 (2004).

[2] M. Barmentlo, G. W. 't Hooft, E. R. Eliel, E. W. M. van der Ham, Q. H. F. Vrehen, A. F. G. van der Meer, and P. W. van Amersfoort, Phys. Rev. A **50**, R14 (1994); E. R. Eliel, E. W. M. van der Ham, Q. H. F. Vrehen, G. W. Hooft, M. Barmentlo, J. M. Auerhammer, A. F. G. van der Meer, and P. W. van Amersfoort, Appl. Phys. A: Mater. Sci. Process. **60**, 113 (1995).

[3] Dennis K. Hore, Mathew Y. Hamamoto, and Geraldine L. Richmond, J. Chem. Phys. **121**, 12589 (2004).

[4] Y. R. Shen, *The Principles of Nonlinear Optics* (Wiley, New York, 1984).

[5] W. G. Spitzer and D. A. Kleinman, Phys. Rev. **121**, 1324 (1961); F. Gervais and B. Piriou, Phys. Rev. B **11**, 3944 (1975).

[6] D. F. Kiselev and L. P. Osipova, Sov. Phys. Crystallogr. **11**, 255 (1966); D. F. Kiselev and L. P. Osipova, *ibid.* **11**, 357 (1966); D. F. Kiselev, *ibid.* **11**, 752 (1966).

[7] J. F. Scott and S. P. S. Porto, Phys. Rev. **161**, 903 (1967); Jon D. Masso, C. Y. She, and D. F. Edwards, Phys. Rev. B **1**, 4179 (1970); V. S. Gorelik and M. M. Sushchinskii, Sov. Phys. Solid State **12**, 1157 (1970); V. J. Tekippe, A. K. Ramdas, and Sergio Rodriguez, Phys. Rev. B **8**, 706 (1973).

[8] Y. R. Shen, Proc. Natl. Acad. Sci. U.S.A. **93**, 12104 (1996).

[9] Y. R. Shen, Annu. Rev. Phys. Chem. **40**, 327 (1989).

[10] X. Gonze, D. C. Allan, and M. P. Teter, Phys. Rev. Lett. **68**, 3603 (1992); P. Umari, A. Pasquarello, and A. Dal Corso, Phys. Rev. B **63**, 094305 (2001).

[11] F. A. Cotton, *Chemical Applications of Group Theory* (Wiley, New York, 1965), Pt. II.

[12] S. Singh, in *Handbook of Lasers*, edited by R. J. Pressley (CRC, Cleveland, OH, 1971), Appendix IIA.